Environmental Science & Technology

pubs.acs.org/est

Article

Negative Pressure Membrane Distillation for Excellent Gypsum Scaling Resistance and Flux Enhancement

Yongjie Liu, Thomas Horseman, Zhangxin Wang, Hassan A. Arafat, Huabing Yin, Shihong Lin,* and Tao He*

Cite This: *Environ. Sci. Technol.* 2022, 56, 1405−1412

Read Online

ACCESS | Metrics & More | Article Recommendations | Supporting Information

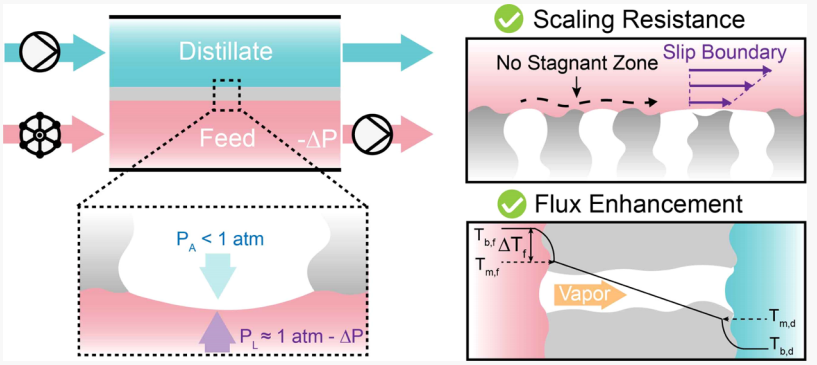

ABSTRACT: Membrane distillation (MD) has potential to become a competitive technology for managing hypersaline brine but not until the critical challenge of mineral scaling is addressed. The state-of-the-art approach for mitigating mineral scaling in MD involves the use of superhydrophobic membranes that are difficult to fabricate and are commercially unavailable. This study explores a novel operational strategy, namely, negative pressure direct contact membrane distillation (NP-DCMD) that can minimize mineral scaling with commercially available hydrophobic membranes and at the same time enhance the water vapor flux substantially. By applying a negative gauge pressure on the feed stream, NP-DCMD achieved prolonged resistance to $CaSO_4$ scaling and a dramatic vapor flux enhancement up to 62%. The exceptional scaling resistance is attributable to the formation of a concave liquid−gas under a negative pressure that changes the position of the water−air interface to hinder interfacial nucleation and crystal growth. The substantial flux enhancement is caused by the reduced molecular diffusion resistance within the pores and the enhanced heat transfer kinetics across the boundary layer in NP-DCMD. Achieving substantial performance improvement in both the scaling resistance and vapor flux with commercial membranes, NP-DCMD is a significant innovation with vast potential for practical adoption due to its simplicity and effectiveness.

KEYWORDS: *membrane distillation, negative pressure, scaling resistance, water−air interface, slip boundary*

INTRODUCTION

Membrane distillation (MD) is a thermally driven desalination process where a microporous hydrophobic membrane acts as a physical barrier of direct liquid transfer between hot feed and cold distillate streams.[1] Due to the transmembrane temperature gradient-induced vapor pressure gradient, water vapor transports through the membrane pores from the feed to the distillate. As the vapor pressure is weakly dependent on feed salinity, MD is an attractive process for hypersaline brine treatment where the osmotic pressure requirements make reverse osmosis inapplicable.[2] Furthermore, the ability to power MD with low-grade heat, such as solar or geothermal energy and waste heat from industrial processes, makes it attractive from a sustainability perspective. Compared to conventional thermal desalination processes like multi-stage flash and multi-effect distillation, the compact modular design of MD makes it more competitive for distributed brine treatment and integration with other modular brine treatment processes.[3,4]

Nevertheless, a big challenge of MD, especially in treating hypersaline brine, is mineral scaling (also referred to as inorganic fouling).[5−7] Scaling occurs when the feed solution is concentrated beyond its solubility limit, which results in mineral precipitation. The precipitated minerals block the membrane pores and reduce the membrane's water vapor

Received: October 19, 2021
Revised: December 13, 2021
Accepted: December 14, 2021
Published: December 23, 2021

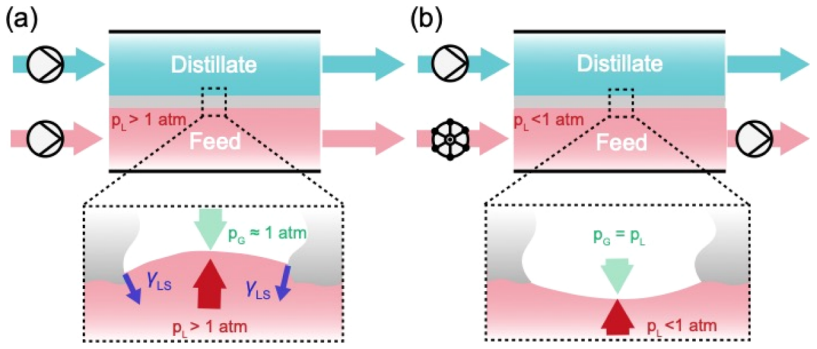

Figure 1. Schematic of DCMD with the (a) positive and (b) negative feed pressure. (a) With a positive feed pressure, the pump is placed upstream of the feed channel to push the solution into the feed channel. The local feed pressure is balanced by both the gas pressure in the pore and the interfacial force exerted by the pore edge. (b) With a negative feed pressure, the pump is placed downstream of the feed channel to pull the solution out of the feed channel. A valve is installed upstream of the cell so that both the flow rate and pressure can be controlled by adjusting the valve and the pump speed. The effective cell dimension was 50 × 20 × 3 mm in length, width, and height for both feed and distillate channels, respectively. The same feed and distillate flow velocity of 0.17 m/s was maintained.

permeability. Scaling by gypsum, silica, calcite, sodium chloride, and mixed salt feed solutions has been investigated.[8−13] Among different types of scalants, gypsum is one of the most challenging and widely studied scalants due to its practical relevance and its low and pH-insensitive solubility, that is, scaling by gypsum cannot be mitigated by merely adjusting the pH of the feed solution as in the case of mitigating calcite scaling.[8,14,15]

In a scaling process, nucleation of mineral precipitates typically occurs via two concurrent pathways: (1) in the bulk solution and (2) heterogeneously on the membrane surface.[16−18] On the one hand, precipitates that nucleate in the bulk solution may deposit on the membrane surface and block the pores, resulting in flux decline and providing potential growth sites for further mineral growth. On the other hand, precipitates that nucleate in the membrane pores (near the surface) not only block the pores but may eventually lead to membrane pore deformation due to crystallization pressure within the membrane pores. Pore deformation often results in membrane pore wetting as the liquid entry pressure (LEP) decreases and the crystals create a pathway for direct liquid feed permeation through the membrane.[14] Both the fouling and wetting mechanisms of scaling can result in complete process failure.[17]

As membrane wetting can be mitigated using omniphobic membranes,[19−21] recent studies have also shown that superhydrophobic membranes are effective for scaling mitigation. Superhydrophobic membranes, sometimes referred to as slippery membranes due to their low sliding angles with water, can delay the onset of mineral scaling or even nearly eliminate scaling in some cases, depending on the scaling species and operation mode.[8,11,15,22,23] For example, superhydrophobic membranes alone were shown to dramatically delay scaling by gypsum and entirely inhibit scaling by sodium chloride.[11,14] When combining superhydrophobic membranes and operational innovations synergistically, even gypsum scaling can be inhibited altogether.[23,24] Furthermore, superhydrophobic membranes have significantly reduced mineral scaling with real industrial wastewaters such as cooling tower blowdown from power plants.[8,25] The scaling resistance can be attributed to the low adhesion, air-filled, superhydrophobic surface that (1) reduces liquid-membrane contact area available for crystal deposition or growth, (2) has a low surface energy and thus a low propensity for heterogeneous nucleation, and (3) introduces a slip boundary condition that inhibits concentration polarization and long residence time for crystal growth and deposition.[17] In most studies, commercial hydrophobic membranes, which lack all these features, were used as a reference for comparison and have consistently shown very poor scaling resistance.

However, superhydrophobic membranes are not commercially available and the fabrication thereof adds cost and complexity to the manufacturing process. Additionally, the fabrication of superhydrophobic membranes often involves the use of per-fluorinated compounds and nanoparticles coating, which raises environmental and health concerns to both manufacturing and the use of such membranes.[15,26−32] Therefore, despite the great promise superhydrophobic membranes have shown to attain scaling resistance, it is practically much more appealing if scaling resistance can be achieved with conventional and commercially available hydrophobic membranes.

In this study, we show that excellent gypsum scaling resistance and flux enhancement can be achieved using conventional commercial hydrophobic membranes with a novel operation mode, namely, negative pressure direct contact membrane distillation (NP-DCMD). Unlike conventional DCMD, in which the feed pump is placed upstream of the feed channel pushing the feed water into the MD cell (or module), the feed pump in NP-DCMD is placed downstream of the feed channel withdrawing water from the MD cell (or module). Consequently, the feed stream in conventional DCMD has a positive gauge pressure (i.e., relative to atmospheric pressure), whereas the feed stream in NP-DCMD has a negative gauge pressure. By performing DCMD experiments with both positive and negative feed (gauge) pressures, we systematically compare the scaling resistance and water vapor flux in these two configurations. We also perform mass and heat transfer modeling to elucidate the mechanism of vapor flux enhancement achieved by NP-DCMD.

MATERIALS AND METHOD

Membranes and Chemicals. A commercial flat-sheet polyvinylidene fluoride (PVDF) hydrophobic membrane (GVHP00010) was purchased from Millipore, USA. The PVDF membrane has been extensively studied in the literature as a benchmark membrane and was fully characterized (as

https://doi.org/10.1021/acs.est.1c07144
Environ. Sci. Technol. 2022, 56, 1405−1412

listed in Table S1, mean pore size = 0.22 μm, thickness = 125 μm, water contact angle = 110°, and LEP = 2.4 bar). Calcium chloride ($CaCl_2$, analytical grade, Sigma-Aldrich) and sodium sulfate (Na_2SO_4, analytical grade, Sigma-Aldrich) were used as received without further purification.

MD with Positive and Negative Feed Stream Pressure. The MD performance of the PVDF membrane under various operating conditions was evaluated using a closed-loop bench-scale MD test unit. To avoid the influence of the pulse flow from the peristaltic pump in the feed loop, a pressure buffer was placed at the inlet of the test cell. A gear pump was used to circulate the distillate, and the conductivity of the distillate was constantly monitored using a conductivity sensor. Figure 1a,b schematically shows the flow direction and the relative position of the pump to create negative and positive gauge pressure in the feed channel of the MD cell.

For controlling the level of negative feed pressure, the feed pump was placed downstream of the MD cell and an adjustable needle valve was used to change the inlet pressure (Figure 1b). By partially closing the valve, a higher degree of vacuum was created in the cell. To compensate for flow rate reduction, the pumping speed was adjusted accordingly. The inlet pressure was monitored using a digital pressure sensor (refer to Figure S1 for a schematic of the DCMD bench-scale experimental setup). The difference between the pressures measured at the inlet and the outlet of the MD cell is negligibly small, which suggests minimum pressure drop within the MD cell. We note that the measured pressure outside the MD cell may not accurately reflect the actual pressure inside the MD cell due to the Venturi effect. We have calculated the flow velocity within the feed and distillate channels based on their cross-sectional areas and used the Bernoulli equation to evaluate the pressure within the channels based on the pressure measured outside the cell. The calculation suggests that the difference between the pressures inside and outside the MD cell is negligibly small because velocity head is negligibly small as compared to the pressure head (Table S2).

When a positive (gauge) pressure is applied on the feed stream (P_L > 1 atm), the feed pressure is balanced by both the gas pressure in the pore (P_G > 1 atm) and the interfacial force (γ_{LS}) imposed by the hydrophobic membrane until LEP is reached (Figure 1a). Specifically, the force balance can be described as $P_L - P_G = 2\gamma_{LS}/a$ with a being the pore radius. When a negative (gauge) pressure is applied on the feed stream (P_L < 1 atm), the interfacial force is negligible as the liquid is not pushed into a hydrophobic pore, and the gas pressure within the pore is approximately the same as the sub-atmospheric feed pressure (Figure 1b).

If the feed pressure is only slightly negative, deformation of the interface toward the feed solution may increase the gas volume in the pore to account for the required vapor reduction, that is, the pore volume V must increase to decrease the total gas pressure P_G according to the ideal gas law $P_G V = nRT$ (where n is the mole of gas in the pores, R is the ideal gas constant, and T is the absolute temperature). However, the deformation of the liquid−gas interface can only occur to a limited extent beyond which non-condensable gases in the pore must be partially removed (i.e., n is reduced) via either dissolution into the feed stream or formation of gas bubbles to be carried away by the flowing feed stream. In other words, the reduction of gas pressure within pores occurs simply because the gas pressure must match the liquid pressure in the feed stream, which differs from the mechanisms of gas pressure reduction in vacuum MD or air-gap MD.[33,34]

Gypsum Scaling Experiments. A 1.2 L $CaSO_4$ feed solution (2000 mg/L, saturation index = 0.09) was prepared and pre-heated to 70 °C before the MD experiments .[23] The feed and distillate streams flowed in a co-current mode. The water vapor flux across the membrane, J (L m^{-2} h^{-1}), was monitored by measuring the distillate mass change over time. Experiments were terminated at a flux decline of 50%. A feed spacer was used to promote turbulence and provide mechanical support to the membrane. The spacer was 1.2 mm thick and was composed of filaments with a diameter of 1 mm, as schematically shown in Figure S2.[35] In addition to performing experiments using commercial PVDF membrane with both positive and negative pressure, we also performed an additional experiment using superhydrophobic membrane with pulse flow, as it is the state-of-the-art method of mitigating gypsum scaling and serves as a benchmark for comparison. The fabrication of the superhydrophobic membrane using micro-pillar templating and CF_4 plasma and the pulse flow operation were detailed in our previous publication (Supporting Information S1.4 and S1.5).[23]

To identify the scalants on the membrane surfaces, the scaled membrane samples were taken out of the test cell, rinsed with deionized water to remove excess feed solution, and dried (the $CaSO_4$ precipitates adhered strongly enough to the membrane and were thus not removed by a gentle rinse). The dried membrane with scalants on the surface was sputter-coated with a thin layer of gold and analyzed via scanning electron microscopy (HITACH TM-1000).

RESULTS AND DISCUSSION

Membrane Wetting Properties. The commercial PVDF membrane exhibited a water contact angle of 110°, but no sliding angle was measured as the drop stayed pinned even on a vertical surface (Table S1). Thus, under zero and positive gauge pressure, liquid intrudes into the membrane pores and the PVDF membrane surface is partially wetted (i.e., the liquid−gas interface is within the pores).[36] Constrained by the pump specifications, the negative feed pressure was limited to a minimum gauge pressure of −30.0 kPa (−0.3 bar), which was far below the LEP of the PVDF membrane (2.4 bar, Table S1) and thus would not induce the penetration of the distillate into the membrane pores. In all the scaling experiments to be discussed below, the distillate conductivity was ∼10 ± 1 μS/cm, which suggests the absence of pore wetting.

Scaling Resistance with Negative Feed Pressure. At a positive feed pressure of 1.0 kPa, the flux of the PVDF membrane quickly declined after 500 mL of distillate was recovered from the feed solution (Figure 2, green triangles), indicating the onset of precipitous gypsum nucleation and deposition of gypsum crystals that blocked the membrane pores. When a superhydrophobic membrane was used in combination with the pulse flow, flux decline was substantially slower after recovering 500 mL of distillate (Figure 2, red circles). This slow flux decline indicates insignificant gypsum scaling, which has been elaborated in our previous study with the support of scanning electron microscopy (SEM) images showing the absence of precipitate on the membrane surface.[23] We showed in the same study that neither the super-hydrophobic membrane nor pulse flow alone could achieve resistance to gypsum scaling and that the synergy between the two factors is critical.[23]

https://doi.org/10.1021/acs.est.1c07144
Environ. Sci. Technol. 2022, 56, 1405−1412

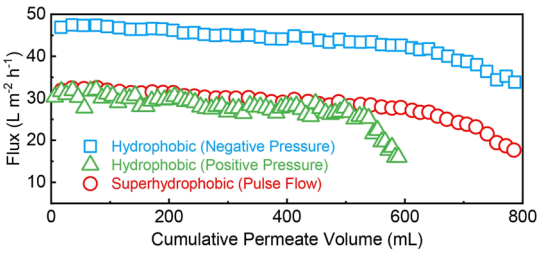

Figure 2. Scaling resistance (to gypsum as the scalant) of a commercial hydrophobic membrane under positive pressure (green triangles, 1.0 kPa), under negative pressure (blue squares, −30.0 kPa), and superhydrophobic (slippery) membrane with pulse flow operation (red circles).[23] The feed solution contained 2000 mg L^{-1} $CaSO_4$ solution (SI = 0.09). The temperatures of the feed solution and distillate were 70 and 20 °C, respectively. The same crossflow velocity of 0.17 m/s was used in both the feed and distillate streams. The experiments were stopped when the cumulative distillate volume reached 800 mL because the feed volume became insufficient for flow circulation. (Reproductive experimental data are given in Supporting Information Figure S3.)

In this study, we observe that the same excellent resistance to gypsum scaling, as achieved using the superhydrophobic membrane with pulse flow, can also be achieved with a conventional hydrophobic membrane and a negative feed pressure of −30.0 kPa (Figure 2, blue squares). Even with a cumulative distillate volume of 800 mL (corresponding to a water recovery over 66%), only a small degree of gradual flux decline was observed possibly due to the reduction of partial vapor pressure at high salinity. At this water recovery, the $CaSO_4$ concentration in the feed solution was above 5000 mg L^{-1} [saturation index (SI) = 0.48] and the solution was far beyond saturation. Surprisingly, the vapor flux was ∼60% higher with operation using negative gauge pressure than that using positive gauge pressure, which will be elucidated in more detail in the following section.

At negative feed pressure, the majority of $CaSO_4$ crystals on the PVDF membrane formed in the regions contacting the spacer (Figure 3a,c,d). Accumulation of crystals next to the spacer filament (Figure 3d) was likely due to the presence of hydrodynamically stagnant regions that favor (1) deposition of mineral precipitates[37,38] and (2) more severe concentration polarization that facilitates nucleation and crystal growth.[39,40] Far from the spacer filament (Figure 3c), where negative feed pressure has greater influence on the shape and position of the liquid−gas interface, significantly fewer crystal precipitates were observed. In contrast, the PVDF membrane operated at a positive feed pressure of 1.0 kPa was fully covered with $CaSO_4$ crystals (Figure 3b,e). These observations confirm the results (e.g., flux decline) from the DCMD experiments that the novel operating strategy using negative feed pressure can effectively mitigate membrane scaling (by gypsum) even if only a commercial hydrophobic membrane is used.

The excellent scaling resistance observed with negative feed pressure on a commercial hydrophobic membrane can be attributed to the influence of the negative feed pressure on the shape and position of the liquid−gas interface (Figure 4). In conventional DCMD with a hydrophobic membrane and a positive feed pressure, the meniscus (i.e., the liquid−gas interface) is convex and the membrane pores are partially wetted near the pore mouths (Figure 4a). This partial intrusion of feed solution, along with the non-slip boundary condition, creates hydrodynamically stagnant zones in the pores near the membrane surface. These stagnant zones exacerbate concentration polarization and increase the residence time for crystal deposition and growth. When a negative feed pressure is applied, however, these stagnant zones and the non-slip boundary conditions no longer exist, as the liquid−gas interface becomes concave and curved into the feed solution (Figure 4b).

The scaling resistance imparted by the concave liquid−gas interface has two possible mechanisms: (1) the concave liquid−gas interface reduces the liquid-membrane contact area available for crystal adhesion and growth and (2) the concave liquid−gas interface introduces a slip boundary condition at the feed solution−membrane interface, which mitigates

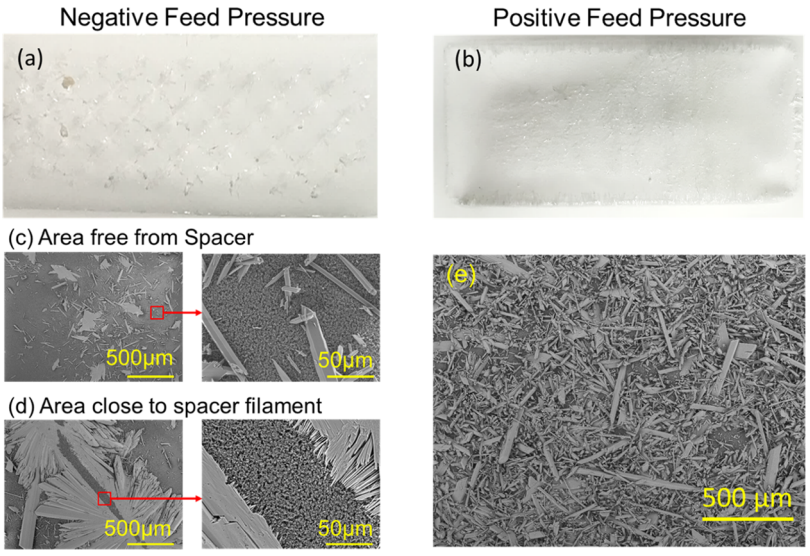

Figure 3. Photographic images of the membrane surface after experiments of (a) NP-DCMD and (b) conventional DCMD. SEM images of the membrane surface after experiments of (c,d) NP-DCMD and (e) conventional DCMD. Specifically, (c) shows the area uncovered by the spacer filament and (d) shows the area covered by or near the spacer filament. All photographic and SEM images were obtained using the commercial hydrophobic membrane (C-PVDF).

https://doi.org/10.1021/acs.est.1c07144
Environ. Sci. Technol. 2022, 56, 1405−1412

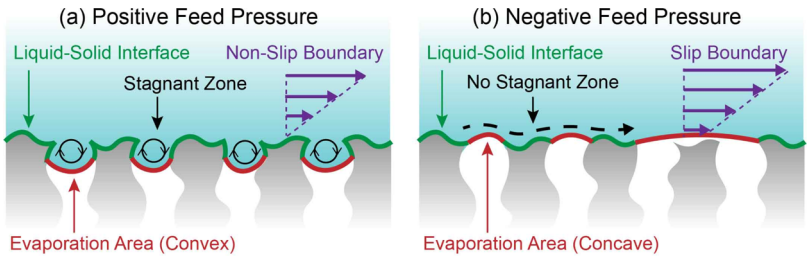

Figure 4. Schematic illustration of the proposed mechanisms for the scaling resistance and enhanced flux. (a) With a positive feed pressure, the meniscus (i.e., water−air interface) is convex, the area for the water−membrane contact is larger, the flow of the feed stream has a non-slip boundary condition, and there are stagnant zones at the entrance of the pores. (b) With a negative feed pressure, the meniscus is concave, the area for the water−membrane contact is smaller, the flow of the feed stream has a slip boundary condition, and there is no stagnant zone near the membrane surface.

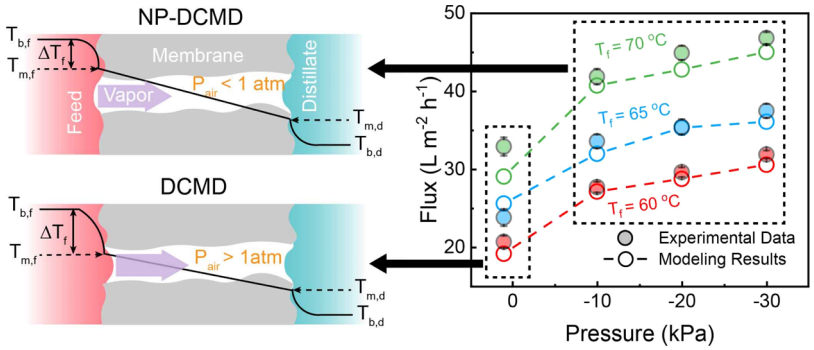

Figure 5. Left: Schematic illustration of temperature distribution T and air pressure in the pores P_{air} in both of DCMD and NP-DCMD. The subscript b, m, f, and d of T denote the bulk, membrane surface, feed, and distillate side, respectively. Right: Vapor flux as functions of feed gauge pressure (1.0 to −30.0 kPa) at 60 °C (red), 65 °C (blue), and 70 °C (green). The filled circles represent the experimental data whereas the empty circles represent the simulated results based on the Dusty-Gas model (shown in Section S4: MATLAB Code of Mass and Heat Transfer in NP-DCMD). The error bar of experimental results is shown in Table S3.

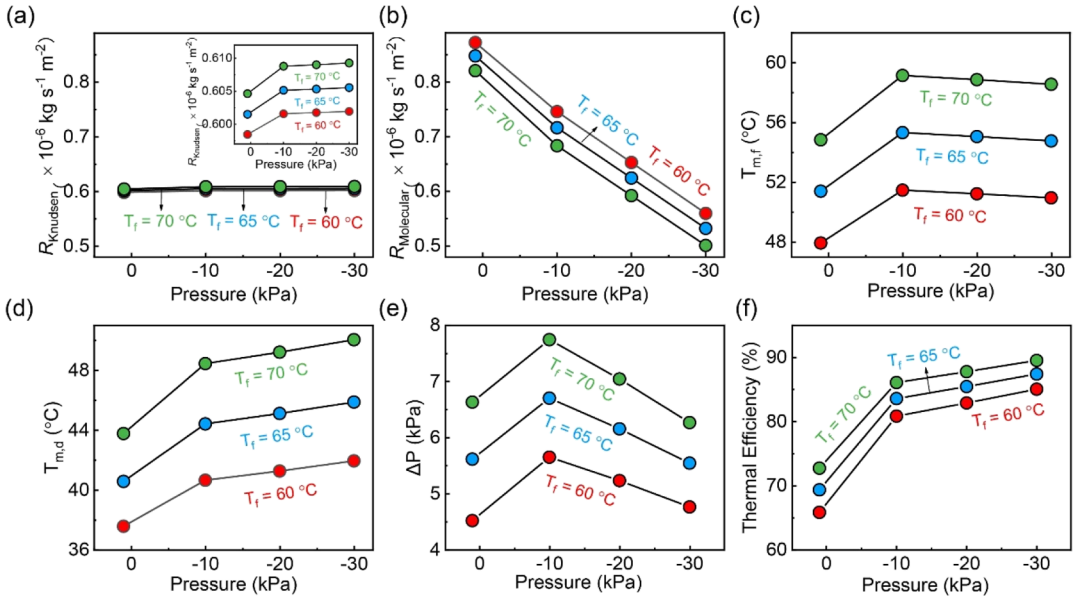

Figure 6. (a) Resistance for Knudsen diffusion. (b) Resistance for molecular diffusion. (c) Temperature at membrane surface contacting the feed stream. (d) Temperature at membrane surface contacting the distillate stream. (e) Water vapor pressure difference across the pores of an MD membrane. (f) Thermal efficiency. All parameters are evaluated for four different feed gauge pressures, including positive (1.0 kPa) and negative (−10, −20 and −30 kPa) pressures, and for three feed bulk temperatures (60, 65 and 70 °C) with distillate bulk temperature maintained at 20 °C.

concentration polarization and decreases the residence time for crystal deposition and growth.[11,41] Both effects possibly have contributed to the scaling resistance of a superhydrophobic membrane (in regular MD) that reduces the convexity of the water−air interface and minimizes the liquid intrusion into pores. However, the concave interface and the complete elimination of pore intrusion in NP-DCMD with hydrophobic membranes are likely even more effective in mitigating mineral

https://doi.org/10.1021/acs.est.1c07144
Environ. Sci. Technol. 2022, 56, 1405−1412

scaling than regular DCMD with superhydrophobic membranes.

Flux Enhancement with Negative Feed Pressure. The initial flux of NP-DCMD was 48.6 L m^{-2} h^{-1}, which was 62% higher than that of conventional DCMD under positive pressure (Figure 2). To better understand this remarkable flux enhancement, the NP-DCMD vapor flux was measured experimentally over a range of feed pressures and temperatures (Figure 5). Water vapor flux increased with decreasing feed pressure at any given feed temperature. Increasing temperature resulted in a nonlinear increase in water vapor flux due to the exponential dependence of water vapor pressure on temperature. We estimated the vapor flux for NP-DCMD using the Dusty-Gas model by considering the effects of temperature and pressure on (1) molecular diffusion resistance, which influenced the membrane permeability coefficient and (2) the heat transfer, which influences the temperature profile, and thus, the partial vapor pressure across the membrane.

To quantify the effect of pore air pressure on vapor transfer resistance, we considered the Knudsen flow and molecular diffusion resistances, which are the two major resistances of vapor transfer through membrane pores in DCMD (model derivations are presented in Section S2: Vapor Transport in MD).[1] The Knudsen resistance increases negligibly with feed pressure and temperature due to the slight increase in the average membrane pore temperature with decreasing feed pressure (eq S2.1, Figure 6a). However, the molecular diffusion resistance decreases dramatically as feed pressure decreases because the negative feed pressure directly reduces the air pressure inside the membrane pores (eq S2.2, Figure 6b), which increases the membrane permeability coefficient, and thus, increases the water vapor flux. In fact, in vacuum enhanced DCMD, where negative gauge pressure is applied to the distillate stream, a similar mechanism for flux enhancement has been proposed.[42] However, the magnitude of flux enhancement predicted based on the changes of Knudsen and molecular diffusion resistances is significantly and consistently less than the experimental observations (Figure S4), which suggests that the impact of negative pressure on enhanced vapor transport alone is insufficient to explain the observed flux enhancement.

Next, the effect of heat transfer on water vapor flux with negative feed pressure was considered. The liquid−gas interface on the feed side of the membrane is convex with a positive feed pressure and concave with a negative feed pressure. The slip boundary induced by the concave meniscus in NP-DCMD results in a larger convective heat transfer coefficient, h_f, relative to that in a regular DCMD process. The enhanced convective heat transfer reduces the feed side temperature polarization and increases the local temperature at the feed solution/membrane interface (eq S3.2, Figure 6c).[43] The concave meniscus also reduces the liquid−solid interfacial area while increasing the liquid−gas interfacial area available for evaporation, decreasing overall conductive heat transfer coefficient of the membrane, h_m (eq S3.4). To account for these differences in heat transfer in NP-DCMD, h_f was multiplied by a correction factor φ_1 which accounts for the enhanced hydrodynamics in the boundary layer and h_m was multiplied by a correction factor φ_2 which accounts for the impact of concave meniscus on conductive heat transfer. In conventional DCMD with positive feed pressure, φ_1 and φ_2 are taken to be unity (i.e., no correction is applied) and the heat transfer coefficients are extracted from fitting the experimental data. Using the same set of parameters extracted from conventional DCMD (except φ_1 and φ_2), we find that φ_1 = 1.7 and φ_2 = 0.7 when a negative feed pressure was applied (more information could be found in Section S3: Detailed Description of Heat Transfer in MD).

Heat transfer has a direct impact on the driving force for vapor transfer. The slip boundary condition and the reduced transmembrane conductive heat transfer, both resulting from the concave liquid−gas interface, contribute to reduced temperature polarization in the feed stream and affect the temperature at the feed/membrane interface, $T_{m,f}$ (Figure 6c), and that at the distillate/membrane interface, $T_{m,d}$ (Figure 6d). The changes in $T_{m,f}$ and $T_{m,d}$ result in the change of vapor pressure difference, which is the driving force for vapor transfer (Figure 6e). While the calculated change of driving force with more negative feed pressure is not monotonic, the observed monotonic increase in flux (Figure 5) is a result of both nonmonotonic variation in driving force and monotonic reduction in vapor transfer resistance. Considering both the impacts of negative pressure on the transmembrane vapor pressure difference (Figure 6e) and the vapor transport resistances (Figure 6a,b), the revised mass transfer for NP-DCMD can accurately explain the experimentally observed flux enhancement (Figure 5).

Lastly, the enhanced vapor flux and reduced conductive heat transfer due to negative feed pressure result in a higher thermal efficiency (Figure 6f), that is, more efficient utilization of driving force for vapor transfer. In other words, NP-DCMD also has extra kinetic (i.e., high vapor flux) and energetic (i.e., higher energy efficiency) benefits in addition to the exceptional scaling resistance. The thermal efficiency achieved using NP-DCMD with a commercial hydrophobic membrane is among the highest in all DCMD processes reported in literature.[44,45]

IMPLICATIONS

Instead of resorting to a complicated membrane design based on multi-step surface modifications with chemical or/and physical approaches, our study demonstrates a much simpler and practically more appealing approach of scaling mitigation using the novel operation strategy of NP-DCMD, which also offers the additional benefit of substantial enhancement of flux and thermal efficiency. The very effective scaling mitigation achieved by NP-DCMD may potentially enable MD to push the limit of water recovery for brine volume minimization or even zero liquid discharge. To reach that goal, more work needs to be performed to understand the effectiveness of NP-DCMD in mitigating other types of scaling, particularly when it is challenged with real feed water with a complex composition.[46,47] In addition, the effectiveness of NP-DCMD for scaling mitigation should also be benchmarked against that of using antiscalants. The combination of NP-DCMD and antiscalants is also worthy of investigation. Moreover, while we can easily control the pressure in a bench-scale system, pressure drop along a full-scale MD module will result in spatial distribution of feed pressure and effectiveness of scaling mitigation. Future research to address these unexplored aspects will further advance NP-DCMD to become potentially the most effective approach for addressing scaling, which is arguably the most critical challenge in MD for high-salinity and high-recovery applications.

https://doi.org/10.1021/acs.est.1c07144
Environ. Sci. Technol. 2022, 56, 1405−1412

■ ASSOCIATED CONTENT

Supporting Information

The Supporting Information is available free of charge at https://pubs.acs.org/doi/10.1021/acs.est.1c07144.

Experimental details for membrane characterization and performance test, vapor transport in MD, detailed description of heat transfer in MD, MATLAB code of mass and heat transfer in NP-DCMD, characteristics of the commercial PVDF and CF_4-MP-PVDF, pressures measured outside the tube and in the feed channel calculated based on the Bernoulli equation, mean value (and standard deviation) water flux at different temperatures and pressures, schematic and photographic image and of the DCMD experimental setup, schematic illustration of the spacer structure, replicate data of the NP-DCMD experiment with a feed solution containing 2000 ppm $CaSO_4$, and simulation results without considering the heat transfer (PDF)

■ AUTHOR INFORMATION

Corresponding Authors

Shihong Lin − *Department of Chemical and Biomolecular Engineering, Vanderbilt University, Nashville, Tennessee 37235-1831, United States; Department of Civil and Environmental Engineering, Vanderbilt University, Nashville, Tennessee 37235-1831, United States;* orcid.org/0000-0001-9832-9127; Email: shihong.lin@vanderbilt.edu

Tao He − *Shanghai Advanced Research Institute, Chinese Academy of Sciences, Shanghai 201210, China;* orcid.org/0000-0002-7566-7649; Email: het@sari.ac.cn

Authors

Yongjie Liu − *Shanghai Advanced Research Institute, Chinese Academy of Sciences, Shanghai 201210, China; Center for Membrane and Advanced Water Technology, Khalifa University, Abu Dhabi 127788, United Arab Emirates*

Thomas Horseman − *Department of Chemical and Biomolecular Engineering, Vanderbilt University, Nashville, Tennessee 37235-1831, United States;* orcid.org/0000-0002-4660-1448

Zhangxin Wang − *Key Laboratory for City Cluster Environmental Safety and Green Development of the Ministry of Education, Institute of Environmental and Ecological Engineering, Guangdong University of Technology, Guangzhou 510006, China; Guangdong Provincial Key Laboratory of Water Quality Improvement and Ecological Restoration for Watershed, Institute of Environmental and Ecological Engineering, Guangdong University of Technology, Guangzhou 510006, China;* orcid.org/0000-0001-6501-3759

Hassan A. Arafat − *Center for Membrane and Advanced Water Technology, Khalifa University, Abu Dhabi 127788, United Arab Emirates;* orcid.org/0000-0002-8616-895X

Huabing Yin − *School of Engineering, University of Glasgow, Glasgow G12 8LT, U.K.;* orcid.org/0000-0001-7693-377X

Complete contact information is available at: https://pubs.acs.org/10.1021/acs.est.1c07144

Notes

The authors declare no competing financial interest.

■ ACKNOWLEDGMENTS

The research was partially supported by National Natural Science Foundation of China (nos. 21978315 and 52011530031), Newton Advanced Fellowship from Royal Society (no. NA170113), CAS International Collaboration (no. GJHZ2080), and US National Science Foundation (no. 1903685). We also thank the framework research consortium for partial financial support (RFBR no. 18-58-80031, NSFC no. 51861145313, DST IPN/7864, NRT no.116020, and CNPq/BRICS-STI-2-442229/2017-8).

■ REFERENCES

(1) Alkhudhiri, A.; Darwish, N.; Hilal, N. Membrane distillation: A comprehensive review. *Desalination* **2012**, *287*, 2−18.

(2) Tong, T.; Elimelech, M. The Global Rise of Zero Liquid Discharge for Wastewater Management: Drivers, Technologies, and Future Directions. *Environ. Sci. Technol.* **2016**, *50*, 6846−6855.

(3) Deshmukh, A.; Boo, C.; Karanikola, V.; Lin, S.; Straub, A. P.; Tong, T.; Warsinger, D. M.; Elimelech, M. Membrane distillation at the water-energy nexus: limits, opportunities, and challenges. *Energy Environ. Sci.* **2018**, *11*, 1177−1196.

(4) Ghaffour, N.; Soukane, S.; Lee, J.-G.; Kim, Y.; Alpatova, A. Membrane distillation hybrids for water production and energy efficiency enhancement: A critical review. *Appl. Energy* **2019**, *254*, 113698.

(5) Naidu, G.; Jeong, S.; Vigneswaran, S.; Hwang, T.-M.; Choi, Y.-J.; Kim, S.-H. A review on fouling of membrane distillation. *Desalin. Water Treat.* **2015**, *57*, 10052−10076.

(6) Warsinger, D. M.; Swaminathan, J.; Guillen-Burrieza, E.; Arafat, H. A.; Lienhard, J. H. Scaling and fouling in membrane distillation for desalination applications: A review. *Desalination* **2015**, *356*, 294−313.

(7) Liu, L.; Xiao, Z.; Liu, Y.; Li, X.; Yin, H.; Volkov, A.; He, T. Understanding the fouling/scaling resistance of superhydrophobic/omniphobic membranes in membrane distillation. *Desalination* **2021**, *499*, 114864.

(8) Karanikola, V.; Boo, C.; Rolf, J.; Elimelech, M. Engineered Slippery Surface to Mitigate Gypsum Scaling in Membrane Distillation for Treatment of Hypersaline Industrial Wastewaters. *Environ. Sci. Technol.* **2018**, *52*, 14362−14370.

(9) Bush, J. A.; Vanneste, J.; Gustafson, E. M.; Waechter, C. A.; Jassby, D.; Turchi, C. S.; Cath, T. Y. Prevention and management of silica scaling in membrane distillation using pH adjustment. *J. Membr. Sci.* **2018**, *554*, 366−377.

(10) Curcio, E.; Ji, X.; Di Profio, G.; Sulaiman, A. O.; Fontananova, E.; Drioli, E. Membrane distillation operated at high seawater concentration factors: Role of the membrane on CaCO3 scaling in presence of humic acid. *J. Membr. Sci.* **2010**, *346*, 263−269.

(11) Xiao, Z.; Zheng, R.; Liu, Y.; He, H.; Yuan, X.; Ji, Y.; Li, D.; Yin, H.; Zhang, Y.; Li, X.-M.; He, T. Slippery for scaling resistance in membrane distillation: A novel porous micropillared superhydrophobic surface. *Water Res.* **2019**, *155*, 152−161.

(12) Mericq, J.-P.; Laborie, S.; Cabassud, C. Vacuum membrane distillation of seawater reverse osmosis brines. *Water Res.* **2010**, *44*, 5260−5273.

(13) Lim, J.; Son, K. P.; Kang, S. M.; Park, J.; Min, S.; Cho, H.; Kim, S.-H.; Lee, S.; Chae, S.; Park, P.-K. Correlation between the feed composition and membrane wetting in a direct contact membrane distillation process. *Environ. Sci.: Water Res. Technol.* **2021**, *7*, 1020−1031.

(14) Christie, K. S. S.; Yin, Y.; Lin, S.; Tong, T. Distinct Behaviors between Gypsum and Silica Scaling in Membrane Distillation. *Environ. Sci. Technol.* **2020**, *54*, 568−576.

(15) Su, C.; Horseman, T.; Cao, H.; Christie, K.; Li, Y.; Lin, S. Robust Superhydrophobic Membrane for Membrane Distillation with Excellent Scaling Resistance. *Environ. Sci. Technol.* **2019**, *53*, 11801−11809.

(16) Tong, T.; Wallace, A. F.; Zhao, S.; Wang, Z. Mineral scaling in membrane desalination: Mechanisms, mitigation strategies, and feasibility of scaling-resistant membranes. *J. Membr. Sci.* **2019**, *579*, 52−69.
(17) Horseman, T.; Yin, Y.; Christie, K. S.; Wang, Z.; Tong, T.; Lin, S. Wetting, Scaling, and Fouling in Membrane Distillation: State-of-the-Art Insights on Fundamental Mechanisms and Mitigation Strategies. *ACS ES&T Engg* **2020**, *1*, 117−140.
(18) Xiao, Z.; Li, Z.; Guo, H.; Liu, Y.; Wang, Y.; Yin, H.; Li, X.; Song, J.; Nghiem, L. D.; He, T. Scaling mitigation in membrane distillation: From superhydrophobic to slippery. *Desalination* **2019**, *466*, 36−43.
(19) Lin, S.; Nejati, S.; Boo, C.; Hu, Y.; Osuji, C. O.; Elimelech, M. Omniphobic Membrane for Robust Membrane Distillation. *Environ. Sci. Technol. Lett.* **2014**, *1*, 443−447.
(20) Boo, C.; Lee, J.; Elimelech, M. Omniphobic Polyvinylidene Fluoride (PVDF) Membrane for Desalination of Shale Gas Produced Water by Membrane Distillation. *Environ. Sci. Technol.* **2016**, *50*, 12275−12282.
(21) Chen, L.-H.; Huang, A.; Chen, Y.-R.; Chen, C.-H.; Hsu, C.-C.; Tsai, F.-Y.; Tung, K.-L. Omniphobic membranes for direct contact membrane distillation: Effective deposition of zinc oxide nanoparticles. *Desalination* **2018**, *428*, 255−263.
(22) Chen, Y.; Lu, K. J.; Chung, T.-S. An omniphobic slippery membrane with simultaneous anti-wetting and anti-scaling properties for robust membrane distillation. *J. Membr. Sci.* **2020**, *595*, 117572.
(23) Liu, Y.; Li, Z.; Xiao, Z.; Yin, H.; Li, X.; He, T. Synergy of slippery surface and pulse flow: An anti-scaling solution for direct contact membrane distillation. *J. Membr. Sci.* **2020**, *603*, 118035.
(24) Horseman, T.; Su, C.; Christie, K. S. S.; Lin, S. Highly Effective Scaling Mitigation in Membrane Distillation Using a Superhydrophobic Membrane with Gas Purging. *Environ. Sci. Technol. Lett.* **2019**, *6*, 423−429.
(25) Robbins, C. A.; Grauberger, B. M.; Garland, S. D.; Carlson, K. H.; Lin, S.; Bandhauer, T. M.; Tong, T. On-site treatment capacity of membrane distillation powered by waste heat or natural gas for unconventional oil and gas wastewater in the Denver-Julesburg Basin. *Environ. Int.* **2020**, *145*, 106142.
(26) Lohmann, R.; Cousins, I. T.; DeWitt, J. C.; Glüge, J.; Goldenman, G.; Herzke, D.; Lindstrom, A. B.; Miller, M. F.; Ng, C. A.; Patton, S.; Scheringer, M.; Trier, X.; Wang, Z. Are Fluoropolymers Really of Low Concern for Human and Environmental Health and Separate from Other PFAS? *Environ. Sci. Technol.* **2020**, *54*, 12820−12828.
(27) Razmjou, A.; Arifin, E.; Dong, G.; Mansouri, J.; Chen, V. Superhydrophobic modification of TiO2 nanocomposite PVDF membranes for applications in membrane distillation. *J. Membr. Sci.* **2012**, *415−416*, 850−863.
(28) Lee, E.-J.; An, A. K.; He, T.; Woo, Y. C.; Shon, H. K. Electrospun nanofiber membranes incorporating fluorosilane-coated TiO2 nanocomposite for direct contact membrane distillation. *J. Membr. Sci.* **2016**, *520*, 145−154.
(29) Zhang, H.; Li, B.; Sun, D.; Miao, X.; Gu, Y. SiO2-PDMS-PVDF hollow fiber membrane with high flux for vacuum membrane distillation. *Desalination* **2018**, *429*, 33−43.
(30) Efome, J. E.; Baghbanzadeh, M.; Rana, D.; Matsuura, T.; Lan, C. Q. Effects of superhydrophobic SiO2 nanoparticles on the performance of PVDF flat sheet membranes for vacuum membrane distillation. *Desalination* **2015**, *373*, 47−57.
(31) Zheng, R.; Chen, Y.; Wang, J.; Song, J.; Li, X.-M.; He, T. Preparation of omniphobic PVDF membrane with hierarchical structure for treating saline oily wastewater using direct contact membrane distillation. *J. Membr. Sci.* **2018**, *555*, 197−205.
(32) Wang, W.; Du, X.; Vahabi, H.; Zhao, S.; Yin, Y.; Kota, A. K.; Tong, T. Trade-off in membrane distillation with monolithic omniphobic membranes. *Nat. Commun.* **2019**, *10*, 3220.
(33) Alsaadi, A. S.; Alpatova, A.; Lee, J.-G.; Francis, L.; Ghaffour, N. Flashed-feed VMD configuration as a novel method for eliminating temperature polarization effect and enhancing water vapor flux. *J. Membr. Sci.* **2018**, *563*, 175−182.
(34) Alsaadi, A. S.; Francis, L.; Maab, H.; Amy, G. L.; Ghaffour, N. Evaluation of air gap membrane distillation process running under sub-atmospheric conditions: Experimental and simulation studies. *J. Membr. Sci.* **2015**, *489*, 73−80.
(35) Yang, C.; Tian, M.; Xie, Y.; Li, X.-M.; Zhao, B.; He, T.; Liu, J. Effective evaporation of CF4 plasma modified PVDF membranes in direct contact membrane distillation. *J. Membr. Sci.* **2015**, *482*, 25−32.
(36) Nagayama, G.; Zhang, D. Intermediate wetting state at nano/microstructured surfaces. *Soft Matter* **2020**, *16*, 3514−3521.
(37) Al-Sharif, S.; Albeirutty, M.; Cipollina, A.; Micale, G. Modelling flow and heat transfer in spacer-filled membrane distillation channels using open source CFD code. *Desalination* **2013**, *311*, 103−112.
(38) Haidari, A. H.; Heijman, S. G. J.; van der Meer, W. G. J. Optimal design of spacers in reverse osmosis. *Sep. Purif. Technol.* **2018**, *192*, 441−456.
(39) Fane, A. G.; Beatson, P.; Li, H. Membrane fouling and its control in environmental applications. *Water Sci. Technol.* **2000**, *41*, 303−308.
(40) Thomas, N.; Sreedhar, N.; Al-Ketan, O.; Rowshan, R.; Abu Al-Rub, R. K.; Arafat, H. 3D printed spacers based on TPMS architectures for scaling control in membrane distillation. *J. Membr. Sci.* **2019**, *581*, 38−49.
(41) Warsinger, D. M.; Tow, E. W.; Swaminathan, J.; Lienhard V, J. H. Theoretical framework for predicting inorganic fouling in membrane distillation and experimental validation with calcium sulfate. *J. Membr. Sci.* **2017**, *528*, 381−390.
(42) Cath, T. Y.; Adams, V. D.; Childress, A. E. Vacuum enhanced direct contact membrane distillation. U.S. Patent US 7,608,188 B2, 2009.
(43) Enright, R.; Hodes, M.; Salamon, T.; Muzychka, Y. Isoflux Nusselt Number and Slip Length Formulae for Superhydrophobic Microchannels. *J. Heat Transfer* **2014**, *136*, 012402.
(44) Zhang, Y.; Peng, Y.; Ji, S.; Li, Z.; Chen, P. Review of thermal efficiency and heat recycling in membrane distillation processes. *Desalination* **2015**, *367*, 223−239.
(45) Leitch, M. E.; Li, C.; Ikkala, O.; Mauter, M. S.; Lowry, G. V. Bacterial Nanocellulose Aerogel Membranes: Novel High-Porosity Materials for Membrane Distillation. *Environ. Sci. Technol. Lett.* **2016**, *3*, 85−91.
(46) Lee, J.-G.; Jang, Y.; Fortunato, L.; Jeong, S.; Lee, S.; Leiknes, T.; Ghaffour, N. An advanced online monitoring approach to study the scaling behavior in direct contact membrane distillation. *J. Membr. Sci.* **2018**, *546*, 50−60.
(47) Fortunato, L.; Jang, Y.; Lee, J.-G.; Jeong, S.; Lee, S.; Leiknes, T.; Ghaffour, N. Fouling development in direct contact membrane distillation: Non-invasive monitoring and destructive analysis. *Water Res.* **2018**, *132*, 34−41.

https://doi.org/10.1021/acs.est.1c07144
Environ. Sci. Technol. 2022, 56, 1405−1412